Letter

Scanning tunneling microscopy of fractional quantum Hall states: Spectroscopy of composite-fermion bound states

Mytraya Gattu [1], G. J. Sreejith [2], and J. K. Jain [1]

[1]*Department of Physics, 104 Davey Laboratory, Pennsylvania State University, University Park, Pennsylvania 16802, USA*

[2]*Indian Institute of Science Education and Research, Pune 411008, India*

(Received 12 December 2023; accepted 10 May 2024; published 22 May 2024)

From the vantage point of an incompressible fractional quantum Hall (FQH) state, an electron injected into it is a complex bound state of an odd number of composite fermions (CFs) dressed by a cloud of particle-hole pairs of CFs, where each CF itself is the bound state of an electron and an even number of quantized vortices. Recent scanning tunneling microscopy experiments provide a spectroscopic probe of the internal energy levels of this bound state, yielding unique information on the short-distance correlations in the FQH liquids. We present detailed calculations showing that the internal energy levels of this bound state, as manifested in the energy-resolved local density of states, depend sensitively on the filling factor and on whether an electron is added or removed. In general, multiple, approximately equally spaced peaks are predicted, with their separation providing a measure of a renormalized CF cyclotron energy. We discuss what aspects of experiments are explained by our model and which ones remain to be explained.

DOI: 10.1103/PhysRevB.109.L201123

A recent breakthrough in performing scanning tunneling microscopy (STM) on fractional quantum Hall (FQH) liquids in graphene [1,2] promises valuable new insights into the microscopic structure of the FQH states [3]. These measurements are made possible by the direct access to graphene, in contrast to the quantum wells which are embedded deep in GaAs heterostructures.

The FQH states are "non-Fermi liquids" of electrons, in that their "elementary particles" (i.e., weakly interacting particles) are not electrons but composite fermions (CFs) [4–7], which are bound states of electrons and an even number ($2p$) of quantized vortices, often pictured as bound states of electrons and $2p$ flux quanta, where a flux quantum is defined as $\Phi_0 = hc/e$. The CFs are distinct from electrons, as evident from the fact that they experience a reduced magnetic field $B^* = B - 2p\rho\Phi_0$ where ρ is the electron (or CF) density. Incompressible ground states occur at filling factors $\nu = n/(2pn+1)$, where CFs fill n CF Landau levels, called Λ levels (ΛLs). A CF excited to a higher ΛL is called a quasiparticle (QP), and a missing CF in a filled ΛL is called a quasihole (QH); each of these carries a fractional charge of magnitude $e/(2pn+1)$ [6]. It is not *a priori* obvious what information STM, which injects an electron into this state, provides.

In the constant height mode, STM measures the tunneling spectral function $A(E)$, or the local density of states (LDOS), given by the sum of $A^+(E)$ and $A^-(E)$, representing electron and hole tunneling into the sample [8–10],

$$A^+(E) = \sum_m |\langle m, N+1|c^\dagger|0,N\rangle|^2 \delta\left(E - E_m^{N+1} + E_0^N\right),$$
$$A^-(E) = \sum_m |\langle m, N-1|c|0,N\rangle|^2 \delta\left(E - E_0^N + E_m^{N-1}\right), \quad (1)$$

where $c^\dagger$ (c) creates (destroys) a localized electron in the lowest Landau level (LLL), $|0,N\rangle$ is the incompressible ground state of N electrons with energy $E_0^N \equiv E_0$, and $|m, N\pm1\rangle$ represents the mth eigenstate of the system with $N\pm1$ electrons with eigenenergy $E_m^{N\pm1}$. The energies will be quoted below relative to the chemical potential μ, which is given, in the thermodynamic limit, by the energy per particle of the incompressible ground state (including the interaction with the background).

From the perspective of the FQH state, the electron (hole) injected by an STM tip is a bound state of $2pn+1$ QPs (QHs) dressed by CF excitons. While the size of the electron/hole is approximately 5–6l_B ($l_B = \sqrt{\hbar c/eB}$ is the magnetic length), QPs and QHs are much larger ($\sim 20 l_B$ at 2/5 [6]), as their size is determined by the effective magnetic length $l_{B^*} = \sqrt{\hbar c/eB^*}$. The STM experiments are a spectroscopic probe of the eigenstates of the multi-QP/QH complex that couple to a localized electron/hole. An early theoretical study predicted a sharp peak in the spectral function for both electron and hole [8]. The recent STM experiments [1] observe more intricate additional structures, which has motivated the present Letter.

An evaluation of the LDOS requires a knowledge of the eigenstates up to high energies. Exact diagonalization (ED) is possible only for systems which are generally too small to bring out the full structure, and ED also will not provide a physical understanding of the results. We proceed by the method of CF diagonalization (CFD) [11], wherein one diagonalizes the Coulomb interaction in the correlated basis of all CF states up to a certain CF kinetic energy (CFKE). This has been shown to provide an excellent representation of the eigenstates of interacting electrons in the FQH liquid (see, for example, Ref. [12]).

We assume below that the physics arises entirely from a single Landau level (LL) which is equivalent to the spin-polarized LLL of GaAs; we thus neglect any form factors arising from the hybridization of spin, valley, or layer degrees of freedom [13]. We do not include the effect of any tip-induced deformation of the FQH liquid and assume that the electron tunnels into a point in a translationally invariant region of the FQH state. Our study also does not consider inelastic tunneling processes involving degrees of freedom, such as phonons, external to the FQH system.

We evaluate the spectral function in the spherical geometry [14], which has N electrons on the surface of a sphere moving under the influence of a radial magnetic field B with a total magnetic flux $2Q\Phi_0$. The kinetic energy of the electrons is quantized into LLs with orbitals in the nth LL ($n = 0, 1, \ldots$) forming an angular momentum multiplet of angular momentum quantum number $l = Q + n$ and can be labeled by the L_z quantum number $-l \leqslant m \leqslant l$. The single-particle orbitals in the nth LL are given by the monopole harmonics $Y_{Q,l,m}(\Omega)$ [15,16] where $\Omega = (\theta, \phi)$ are the coordinates on the surface of the sphere. In particular, the $n = 0$ LL orbitals are given by $Y_{Q,Q,m} \sim u^{Q+m} v^{Q-m}$ where $u = \cos(\theta/2)\exp(\imath\phi/2)$ and $v = \sin(\theta/2)\exp(-\imath\phi/2)$. Jain's CF wave function for the incompressible state at filling $\nu = n/(2pn+1)$ is given by [4,6]

$$\Psi_{\nu=\frac{n}{2pn+1}} = P_{\mathrm{LLL}}\phi_n \prod_{i<j}(u_i v_j - v_i u_j)^{2p}, \tag{2}$$

where ϕ_n is the Slater determinant corresponding to the incompressible integer quantum Hall (IQH) state with n filled LLs on a sphere with $2Q^\star = 2Q - 2p(N-1)$ flux passing through it. P_{LLL} projects the wave function into the $n = 0$ LL, which we implement by the method in Refs. [17,18]. A single QH (QP) can be constructed by replacing ϕ_n by a state containing a single hole in the nth LL (particle in the $n+1$th LL). Neutral excitons are made of QP-QH pairs.

Hole. Tunneling of an electron out of the FQH system creates a hole. For the Jain fractions $\nu = n/(2pn+1)$, the state with a hole at a point, say the north pole $\Omega = \omega = (u = 1, v = 0)$ has quantum numbers $L = Q, L_z = -Q$ and is given by

$$\begin{aligned} c_\omega \Psi_{\frac{n}{2pn+1}}(\Omega_1, \ldots, \Omega_N) &\propto \Psi_{\frac{n}{2pn+1}}(\Omega_1, \ldots, \Omega_{N-1}, \omega) \\ &= P_{\mathrm{LLL}} \prod_{i<j=1}^{N-1} (u_i v_j - v_i u_j)^{2p} \phi_n(\Omega_1, \ldots, \Omega_{N-1}, \omega) \prod_{j=1}^{N-1} v_j^{2p}, \end{aligned}$$

where c_ω annihilates an electron at ω, the north pole. The resulting state is in the CF form, i.e., it is the LLL projection of a wave function containing a Jastrow factor. It can be represented exactly as the linear combination of a finite number of simple CF states, referred to as the minimal basis, with $2pn+1$ QHs clustered near the north pole [see Sec. VI of Supplementary Material (SM) [19] and Ref. [20] therein]. The minimal bases for $\nu = 1/3$ and $\nu = 2/5$ are schematically shown in Figs. 1 and 2 (the explicit basis function can be constructed in the standard manner—by writing the corresponding IQH wave function, multiplying by the Jastrow factor, and then projecting into the LLL), along with the CFKE relative to the minimum CFKE basis function. (At $\nu = 2/5$, one combination of these states occurs at an L different from the L of the hole state, leaving only three basis functions.) These figures also show how a larger CF basis can be constructed by adding CF excitons. The dimension of the minimal basis is independent of N but increases rapidly with n along the sequence $\nu = n/(2pn+1)$ (Sec. VI of SM [19]).

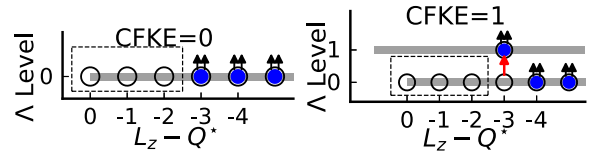

FIG. 1. Left panel: The minimal basis for a hole at $\nu = 1/3$ enclosed by a dashed box. Right panel: A typical configuration of a basis state with unit CF kinetic energy (CFKE). Here and in the following figures the horizontal lines represent the Λ levels, and the CFs are shown as blue dots decorated by two flux quanta (arrows). The spherical geometry is assumed, where L_z is the angular momentum of the orbital and Q^* is the monopole strength experienced by CFs.

CFD in the minimal basis produces approximate eigenstates along with their spectral weights. A comparison with exact diagonalization in small systems validates this minimal basis for spectral function calculation (Sec. IV of SM [19]). We also perform CFD within an enlarged basis that also contains states with additional excitons. We find that these do not produce new peaks but cause a broadening of the peaks at the corresponding CFKE. The hole peak at $\nu = 1/3$ is not broadened.

Figure 3 shows the spectral function on the hole side ($E < \mu$) shaded in green. The energy of each peak and its

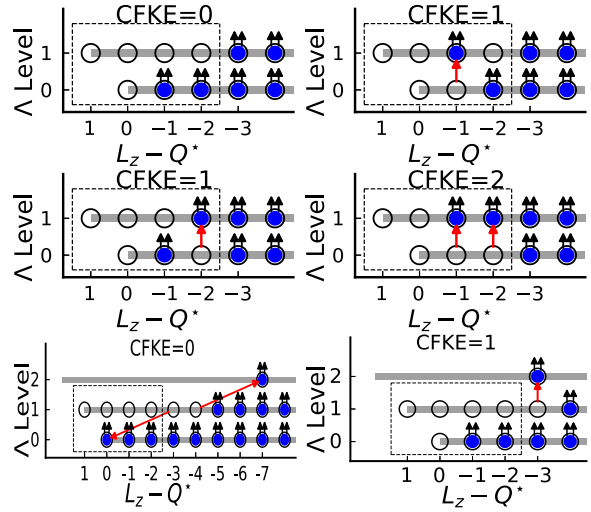

FIG. 2. The top four panels depict the minimal basis that fully captures the hole added to the incompressible state at $\nu = \frac{2}{5}$. The red arrows indicate how these states are obtained starting from the minimum energy state (top left). All excitations are confined to a localized region depicted by the dashed box. The bottom two panels give examples of CF basis states beyond the minimal basis. Their inclusion in CFD broadens the delta function peaks of the minimal basis.

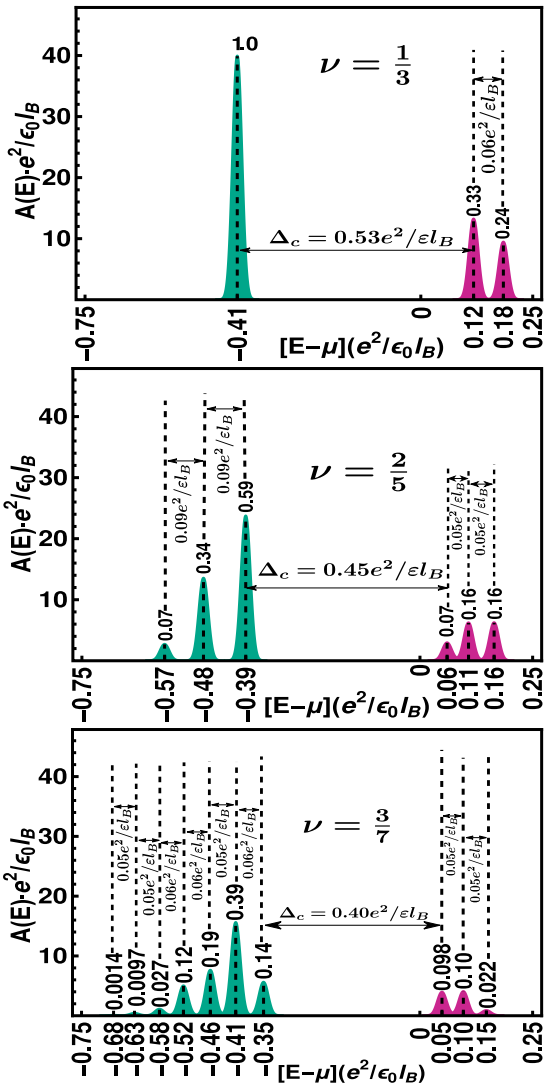

FIG. 3. The spectral function $A(E)$ for $\nu = \frac{1}{3}, \frac{2}{5}$, and $\frac{3}{7}$ calculated using CF theory. The energy is measured in units of $e^2/\epsilon l_B$, where ϵ is the dielectric constant, measured relative to the chemical potential μ. With the exception of the electron side ($E > \mu$) of $\nu = 3/7$, the energy and the spectral weight under each peak (shown near its top) represents the thermodynamic value (obtained by extrapolation [19]). The heights of the peaks are proportional to their spectral weights. For ease of viewing, we have substituted the δ function in Eq. (1) by a normal distribution of width $0.01e^2/\varepsilon l_B$. For $E > \mu$ at $\nu = \frac{3}{7}$, results are shown for a system of $N = 34$ particles; the spectral weights are even smaller in the thermodynamic limit.

integrated spectral weight, shown on the figure, are thermodynamic values estimated from CFD (Sec. IV of SM [19]). The spectral weights add to unity. The line shapes of the peaks are schematic; for some cases, the line shapes obtained from CFD are shown in Sec. IV of SM [19].

Electron. We obtain the electron spectral function by performing CFD within a restricted but sufficiently large CF basis that allows us to reliably identify the resonant energy levels as well as their tunneling spectral weights. The state with an electron added at the north pole (with quantum numbers

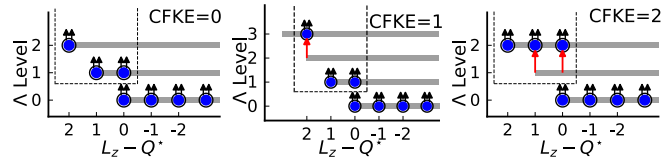

FIG. 4. Examples of CF configurations used to represent an electron at $\nu = \frac{1}{3}$. We consider different configurations of CFs in the dashed region.

$L = L_z = Q$) is given by [8]

$$c_\omega^\dagger \Psi_{\frac{n}{2pn+1}}(\Omega_1, \ldots, \Omega_N) \propto \mathrm{A}\big[Y_{Q,Q,Q}(\Omega_{N+1} = \omega)\Psi_{\frac{n}{2pn+1}}(\Omega_1, \cdots, \Omega_N)\big]. \quad (3)$$

This does not have a CF form, because prior to LLL projection, each term in the antisymmetrized sum contains a Jastrow factor $\prod_{i<j=1}^{N}(u_i v_j - v_i u_j)^{2p}$ that does not include all $N+1$ particles. The electron state thus cannot be exactly represented as a linear superposition of states with a simple CF structure. We proceed by constructing a CF basis which satisfies the following: (i) The lowest n ΛLs are fully occupied, (ii) there is an upper cutoff on the total CFKE, (iii) there is a cutoff on the ΛL index, and (iv) the total angular momentum quantum numbers are $L = L_z = Q$. Consider for example $\nu = 1/3$, shown in Fig. 4. With a net CFKE $\leqslant 2$ and ΛL index $\leqslant 3$, a basis of 16 CF configurations is obtained, some of which are shown in Fig. 4. The calculated $A^+(E)$ has two peaks, shown in Fig. 3, where the energy of each peak and its weight are thermodynamic estimations (see SM [19]). Note that the weights do not add to one—we speculate that the remainder is distributed in a smooth high-energy tail. This indicates a fundamental asymmetry between the additions of a hole and an electron in a FQH system. Figure 5 shows what the density

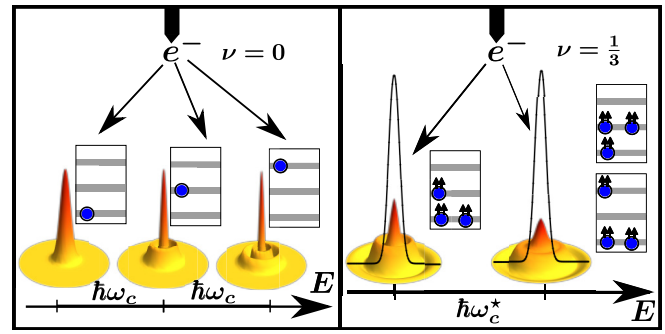

FIG. 5. The left panel shows the density profile of the final state of an electron tunneling into an empty LL. (The states are shown schematically in rectangular boxes.) The right panel shows the density profile (relative to the uniform density ground state) of the final state of an electron tunneling into the 1/3 FQH state for each of the two peaks in Fig. 3. (In the right panel, the density has been multiplied by a factor of 2 for clarity, and the black curve shows the density profile of an electron tunneling into an empty LLL.) The configurations of the excited CFs that contribute most significantly to the two peaks are also shown schematically. The radius of each disk is $\sim 9l_B$.

profiles of the added electron look like for the two peaks at $\nu = 1/3$.

Qualitative understanding of the results. The spectral functions shown in Fig. 3 represent the principal result of our study. To gain insight into its features, we consider a model where the CFs are taken as noninteracting. Within this model the energies can be expressed in terms of the ν-dependent CF cyclotron energy $\hbar\omega^*_\nu$. For example, the separation between the first electron and the first hole peaks is given by $4\hbar\omega^*_{1/3}$ at $\nu = 1/3$ and $8\hbar\omega^*_{2/5}$ for $\nu = 2/5$, and the separation between the peaks within the electron or the hole spectral function is $\hbar\omega^*_\nu$. While this captures the qualitative features, all these energies are renormalized by the inter-CF interaction, which is significant here given the physical proximity of the excited CFs. The peaks are approximately equally spaced for the electron and also for the hole, making it meaningful to identify the separation with a renormalized $\hbar\omega^*_\nu$. Note that the renormalized $\hbar\omega^*_\nu$'s for the electron and the hole sides are not equal at a given ν. On intuitive grounds, one expects that the CF cyclotron energy on the hole side should be larger than that on the electron side because the local B^* for the hole is larger due to the reduced density; this is consistent with the behavior seen in Fig. 3. The multiple peaks thus reflect the ΛL structure that is renormalized by the residual interaction between the CFs. This understanding can be extended to other fractions not accessible to detailed theoretical study.

$\nu = n/(2n-1)$ *FQH states.* On account of the particle-hole symmetry of the problem within a LL, the spectral function for the electron (hole) tunneling into a state at $\nu = 1 - n/(2pn+1)$ is identical, modulo a rigid shift in the energy, to that for the hole (electron) tunneling into a state at filling $\nu = n/(2pn+1)$.

Comparison with experiment. A number of aspects that might be relevant in experiments are not included in our model. The effects of disorder and LL mixing, screening of the interaction by the backgate, and the role of spin are neglected, and it is assumed that the influence of the STM tip's potential on the FQH state is negligible. (We have considered the effect of screening in SM [19], and find that it does not affect the results significantly so long as the screening length is large compared to the size of the electron wave packet. For completeness, we have also evaluated the dependence on finite thickness, which may be relevant for FQH liquids in semiconductor quantum wells, using a model interaction proposed in Ref. [21].) With this caveat, let us consider how the above results compare to the experiment of Ref. [1].

In Ref. [1], the behavior for hole (electron) at $n/(2n+1)$ does not match with that for the electron (hole) at $1 - n/(2n+1)$. Much more structure is seen for $\nu > 1/2$ than for $\nu < 1/2$. This underscores the importance of LL mixing, which breaks particle-hole symmetry. Why LL mixing is more significant for $\nu < 1/2$ is an important question, which very likely involves subtle physics that is beyond the scope of the current Letter.

Experiments do see sharp peaks, as expected from above discussion and from previous studies [8]. On the electron side of $\nu = 2/3$, there is a sharp peak (see Fig. 3(b) of Ref. [1]), which we identify with the single peak on the hole side at $\nu = 1/3$ (Fig. 3). An additional structure is seen on the electron side of $\nu = 2/3$ including a broad peak, the origin of which is unclear. On the hole side of 2/3 there is a sharp peak with a shoulder, which could be two unresolved peaks, as expected from Fig. 3. For the hole side of 2/5, or the electron side of 3/5, we expect three peaks, which may be consistent with experiments (see Fig. 3(b) of Ref. [1]). On the hole side of 3/5, our study predicts three peaks with a small weight; experimentally, a broad peak is seen with a smaller weight.

For a more quantitative comparison, we note that the separation between the closest electron and hole peaks is approximately $0.53\, e^2/\epsilon l_B$ and $0.45\, e^2/\epsilon l_B$ for $\nu = 1/3$ and $\nu = 2/5$. Assuming $\epsilon = 3.5\epsilon_0$ and $B = 14$ T, this translates into 29 and 24 meV. Experimentally, the separation is $\sim$16 meV for $\nu = 2/3$ and $\sim$12 meV for $\nu = 3/5$. The separation between the peaks on the electron side of $\nu = 3/5$ is on the order of $\sim$3 meV in experiments, which corresponds to $0.054\, e^2/\epsilon l_B$. This is to be compared to the theoretical separation of $0.09\, e^2/\epsilon l_B$. While the origin of the factor of $\sim$2 discrepancy between the theoretical and experimental gaps is not known at present, we note that a similar level of mismatch exists for various gaps for the FQHE states in GaAs, often attributed to LL mixing and disorder. At this stage, it is not possible to tell in experiments how the renormalized $\hbar\omega^*_\nu$'s differ on the hole and the electron sides.

Theoretically, we expect weaker peaks on the electron side of $\nu = n/(2n+1)$ or the hole side of $\nu = 1 - n/(2n+1)$. This appears to be the case as seen in Fig. 3(a) of Ref. [1].

Finally, while multiple peaks arise fundamentally from the fractionalization of an electron into an odd number of CFs, these cannot be used to deduce the fractional braiding statistics of the QPs/QHs [22,23], which is well defined only when the separation between QPs/QHs is large compared to their size [24–27]. It has been proposed that disorder-mediated tunneling can help reveal the fractional statistics through STM [9] and that the STM signals contain signatures of entanglement in the FQH phase [10].

Note added. Recently, we became aware of an independent study by Pu *et al.* [28] which has a significant overlap with our work.

Acknowledgments. We are grateful to Ali Yazdani for numerous insightful discussions on STM of FQHE, which motivated the present work. We thank Ajit C. Balram, Songyang Pu, and Z. Papic for pointing out certain quantitative errors in the spectral weights in Ref. [8], which we have also confirmed. M.G. and J.K.J. acknowledge financial support from the U.S. National Science Foundation under Grant No. DMR-2037990. G.J.S. thanks Ashish Arora and Biswajit Karmakar for useful discussions. G. J. S. acknowledges TIFR, Mumbai and JQI and CMTC, University of Maryland for their hospitality during the completion of this work.

[1] Y. Hu, Y.-C. Tsui, M. He, U. Kamber, T. Wang, A. S. Mohammadi, K. Watanabe, T. Taniguchi, Z. Papic, M. P. Zaletel, and A. Yazdani, High-resolution tunneling spectroscopy of fractional quantum Hall states, arXiv:2308.05789.

[2] G. Farahi, C.-L. Chiu, X. Liu, Z. Papic, K. Watanabe, T. Taniguchi, M. P. Zaletel, and A. Yazdani, Broken symmetries and excitation spectra of interacting electrons in partially filled Landau levels, Nat. Phys. **19**, 1482 (2023).

[3] D. C. Tsui, H. L. Stormer, and A. C. Gossard, Two-dimensional magnetotransport in the extreme quantum limit, Phys. Rev. Lett. **48**, 1559 (1982).

[4] J. K. Jain, Composite-fermion approach for the fractional quantum Hall effect, Phys. Rev. Lett. **63**, 199 (1989).

[5] J. K. Jain, Incompressible quantum Hall states, Phys. Rev. B **40**, 8079 (1989).

[6] J. K. Jain, *Composite Fermions* (Cambridge University Press, New York, 2007).

[7] *Fractional Quantum Hall Effects New Developments*, edited by B. I. Halperin and J. K. Jain (World Scientific, Singapore, 2020).

[8] J. K. Jain and M. R. Peterson, Reconstructing the electron in a fractionalized quantum fluid, Phys. Rev. Lett. **94**, 186808 (2005).

[9] Z. Papić, R. S. K. Mong, A. Yazdani, and M. P. Zaletel, Imaging anyons with scanning tunneling microscopy, Phys. Rev. X **8**, 011037 (2018).

[10] S. Pu, A. C. Balram, and Z. Papić, Local density of states and particle entanglement in topological quantum fluids, Phys. Rev. B **106**, 045140 (2022).

[11] S. S. Mandal and J. K. Jain, Theoretical search for the nested quantum Hall effect of composite fermions, Phys. Rev. B **66**, 155302 (2002).

[12] A. C. Balram, A. Wójs, and J. K. Jain, State counting for excited bands of the fractional quantum Hall effect: Exclusion rules for bound excitons, Phys. Rev. B **88**, 205312 (2013).

[13] E. McCann and V. I. Fal'ko, Landau-level degeneracy and quantum Hall effect in a graphite bilayer, Phys. Rev. Lett. **96**, 086805 (2006).

[14] F. D. M. Haldane, Fractional quantization of the Hall effect: A hierarchy of incompressible quantum fluid states, Phys. Rev. Lett. **51**, 605 (1983).

[15] T. T. Wu and C. N. Yang, Dirac monopole without strings: Monopole harmonics, Nucl. Phys. B **107**, 365 (1976).

[16] T. T. Wu and C. N. Yang, Some properties of monopole harmonics, Phys. Rev. D **16**, 1018 (1977).

[17] J. K. Jain and R. K. Kamilla, Composite fermions in the Hilbert space of the lowest electronic Landau level, Int. J. Mod. Phys. B **11**, 2621 (1997).

[18] J. K. Jain and R. K. Kamilla, Quantitative study of large composite-fermion systems, Phys. Rev. B **55**, R4895 (1997).

[19] See Supplemental Material at http://link.aps.org/supplemental/10.1103/PhysRevB.109.L201123 for a discussion of the single QP and QH excitations, details of the spectral weights for different finite systems, and a proof that a localized hole can be fully described by the minimal basis.

[20] J. K. Jain, Theory of the fractional quantum Hall effect, Phys. Rev. B **41**, 7653 (1990).

[21] F. C. Zhang and S. Das Sarma, Excitation gap in the fractional quantum Hall effect: Finite layer thickness corrections, Phys. Rev. B **33**, 2903 (1986).

[22] B. I. Halperin, Statistics of quasiparticles and the hierarchy of fractional quantized Hall states, Phys. Rev. Lett. **52**, 1583 (1984).

[23] D. Arovas, J. R. Schrieffer, and F. Wilczek, Fractional statistics and the quantum Hall effect, Phys. Rev. Lett. **53**, 722 (1984).

[24] H. Kjønsberg and J. Myrheim, Numerical study of charge and statistics of Laughlin quasiparticles, Int. J. Mod. Phys. A **14**, 537 (1999).

[25] H. Kjønsberg and J. M. Leinaas, Charge and statistics of quantum Hall quasi-particles. A numerical study of mean values and fluctuations, Nucl. Phys. B **559**, 705 (1999).

[26] G. S. Jeon, K. L. Graham, and J. K. Jain, Fractional statistics in the fractional quantum Hall effect, Phys. Rev. Lett. **91**, 036801 (2003).

[27] G. S. Jeon, K. L. Graham, and J. K. Jain, Berry phases for composite fermions: Effective magnetic field and fractional statistics, Phys. Rev. B **70**, 125316 (2004).

[28] S. Pu, A. C. Balram, Y. Hu, Y.-C. Tsui, M. He, N. Regnault, M. P. Zaletel, A. Yazdani, Z. Papi, Fingerprints of composite fermion lambda levels in scanning tunneling microscopy, arXiv:2312.06779.